CHARACTERISTICS OF POOL FIRE BURNING

by

Anthony Hamins, Takashi Kashiwagi,
Building and Fire Research Laboratory
National Institute of Standards and Technology
Gaithersburg, MD 20899
and
Robert R. Burch
Dow Corning Corp.
Auburn, MI 48611

Reprinted from Fire Resistance of Industrial Fluids, June 20, 1995, Indianapolis, IN. Proceedings. ASTM STP 1284. American Society for Testing and Materials (ASTM), Philadelphia, PA. Totten, G.E., Reichel, J., Editors. 1996.

Anthony Hamins,[1] Takashi Kashiwagi,[2] and Robert R. Buch[3]

CHARACTERISTICS OF POOL FIRE BURNING

REFERENCE: Hamins, A., Kashiwagi, T., and Buch, R., "**Characteristics of Pool Fire Burning**", Fire Resistance of Industrial Fluids, ASTM STP 1284, George E. Totten and Jurgen Reichel, Eds. American Society for Testing and Materials, Philadelphia, 1995.

ABSTRACT: The structure and energetics of hydrocarbons burning in a pool fire configuration are reviewed. Examples of non-hydrocarbons are also presented. The character and structure of pool fires are discussed with special regard to the flame shape, flame pulsation frequency, flame height, and the detailed flame structure. An enthalpy balance about the flame considers enthalpy losses to the surroundings due to radiation, convection of sensible heat, and combustion efficiency considerations. The power radiated from a flame as a function of burner diameter is discussed. An enthalpy balance about the pool surface partitions the heat feedback into conduction, convection, and radiation. This enthalpy is part of a positive feedback loop which goes to vaporize the fuel. Differences between field and zone models are discussed.

KEYWORDS: burning rate, flame height, pool fire, radiative heat transfer

---

INTRODUCTION TO THE CHARACTER AND STRUCTURE OF POOL FIRES

Many common fire scenarios can be classified as pool fires. These include fires ranging in size from a cigarette lighter, where D is approximately 10^{-3} m, to a forest fire, where D can be as large as 10^{5} m. A pool fire is defined as a buoyant diffusion flame in which the fuel is configured horizontally. Although the name implies that the fuel is a liquid, it may be a gas or a solid. The fuel bed may be of an arbitrary geometry, but for simplicity, most studies consider a circular configuration characterized by a single geometrical scale, the pool diameter (D). Beyond obvious differences in length scale, fire hazard can be characterized in terms of the combustion kinetics of a fuel such as resistance to suppression, flash point temperature, or lower flammability limits, or in terms of heat transfer during combustion, which can be characterized by the total heat release rate, the flame spread rate, or the power radiated to the surroundings. Fire hazard can be modified by ambient conditions such as the absence or presence of an enclosure, a hot surface, wind, currents, or ventilation. These

---

[1]Mechanical Engineer, Building and Fire Research Laboratory (BFRL), National Institute of Standards and Technology, Gaithersburg, MD 20899

[2]Group Leader and Research Scientist, Material Flammability Group, BFRL, National Institute of Standards and Technology, Gaithersburg, MD 20899

[3]Senior Research Specialist, Dow Corning Corp., Auburn, MI 48611

conditions play a role in governing both the detailed structure and the overall hazard of a fire. For a comprehensive review of pool fires including enclosure effects the reader is directed to the excellent review on the topic by Hall [1] and Blinov and Khudyakov [2]. This paper focusses on the structure and character of a pool fire burning in a quiescent environment with an emphasis on mass vaporization and heat release rates. Recent aspects of research in this field are summarized.

Flame Character and shape

When the mass burning rate of a flame exceeds a certain value, the flow field ceases to be laminar. As the mass burning rate continues to increase, the flow field changes from buoyancy to momentum dominated. Accidental liquid spills which result in a pool fire are almost always buoyancy dominated and are typically turbulent.

It is commonly accepted that the larger the fuel supply rate, the larger the heat release rate, and the larger the flame height. Historically, the modeling of pool fires has been based on the assumption that flame dynamics are similar regardless of fire size or fuel type. Pool fire Froude modeling suggests that the ratio of inertia to buoyant forces are the key in simulating the fluid dynamic aspects of pool fires and that chemistry plays a secondary role. Froude modeling has been a common thread used to develop simple models for flame height, pulsation frequency, and mass burning rates in pool fires.

The gross structure of a turbulent buoyant fire can be described in terms of three regions; a fuel rich core known as the persistent zone, an intermittent region with a time varying visible flame tip, and a downstream plume region [3]. The fuel rich core and the plume regions can be thought of as approximately non-reacting, whereas the majority of the heat release occurs in the intermittent region. The fuel rich core is the region just above the fuel surface where little oxygen has penetrated [4]. This region, nominally 20% of the average flame height, is relatively cool and rich in fuel and pyrolysis intermediates [5]. Large scale vortices roll into the fire, entrain air, and define the boundaries of the fuel rich core. Above the fuel rich core is the intermittent region where air is convected radially into the fire. Heat is released as the pyrolysis intermediates react with the entrained air, yielding combustion intermediates, such as carbon monoxide (CO) and soot particles, and combustion products such as water vapor and carbon dioxide. In the fire plume, the rate of chemical reactions decrease exponentially as the temperature drops and more cold air is entrained. Some combustion intermediates like soot or CO may escape the intermittent region into the plume, where temperatures are often too low to completely oxidize these species.

The structure and shape of flames is important in understanding the near field distribution of emitted radiation [6,7]. In general, flame shapes change with time through a pulsation cycle. Often, the time-averaged shape of turbulent fires is taken as approximately either cylindrical or cone-like with the bottom taken as the pool diameter and the top given by the visible flame height. Empirical results by Orloff and de Ris [6,7] have shown that a simple relation adequately describes the time-averaged flame shape over a range of moderate pool diameters (0.1 to 0.7 m), fuel types, and fuel flow rates. Their expression generates a hyperbolic-like curve which replicates the "necking-in" of the flame edge near the pool base which is due to lateral entrainment, and the downstream cresting at the visual flame tip. The lateral extent of the flame boundary at the necking-in region is related to the Froude number. For liquid pool fires, the smaller the Froude number, the more organized the flame structure and the larger the time varying lateral change in the amplitude of the flame boundary at the necking-in region.

The Froude number (Fr) is defined as the ratio of inertial to buoyant forces:

$$Fr = V^2/(L \cdot g) \qquad (1)$$

where g (9.8 m/s^2) is the gravitational acceleration, V is a characteristic velocity, often taken as the (gas phase) fuel velocity at the burner exit and L is a characteristic length scale, often taken as the pool diameter. For $Fr >> 1$, the flow field is momentum dominated, whereas for $Fr << 1$, the flow field is buoyancy dominated.

Pulsation Frequency

A large number of experimental, theoretical and scaling studies have investigated the coherent vortical structures which are shed by flames. This phenomenon has been documented for a wide range of burner diameters, heat release rates, Reynolds numbers and fuel types [8-28]. The vortical structures and their shedding frequency influence the rate of air entrainment into a fire [8]. The pulsing nature of the flow field propagates downstream leading to the time varying flame length which is observed in turbulent fires.

Chen et al. [29] employed flow visualization in buoyant diffusion flames to study the large torroidal vortices which give rise to the flame bulges which are seen as flame pulsations. Experimental studies of the pulsation frequency have utilized various measurement techniques including acoustic detection, hot wire anemometry, fast photography, video, photoelectronic devices, and local temperature and velocity measurements. Typically, these measurements have been correlated with physical dimensions such as the burner surface area [13] or diameter [27].

Buckmaster and Peters [30] suggested that flame pulsations were due to a modified Kelvin-Helmholtz instability. Bejan [31] based his analysis on the buckling theory of inviscid streams and predicted a vortex shedding frequency in qualitative agreement with experimental results. Hertzberg et al. [32] used an order of magnitude analysis to relate the pulsation frequency to the flame speed of a near limit fuel-air mixture propagating from the fire edge towards the axis of the burner.

Emori and Saito [33] emphasized the importance of the Strouhal and Froude numbers in a dimensional analysis of the pulsation frequency of pool fires. The Strouhal number (S) is a non-dimensional frequency defined as:

$$S = f \cdot L/V \qquad (2)$$

where L is a characteristic length (often taken as the burner diameter) and V is a characteristic velocity (often taken as the velocity of the fuel at the burner duct).

Putnam [34] suggested that an empirical dependence exists between S and Fr, although a quantitative analysis of this relationship was not provided. The Strouhal number plotted as a function of the inverse Froude number shown in Fig. 1 correlates the pulsation measurements taken from the literature for flames burning gaseous, liquid and solid fuels over 14 orders of magnitude in Froude number and covering a range of diameters from 0.007 to 50 m [28]. A power law fit to the data yields: $S \propto Fr^{-0.57}$. A power law fit with $S \propto Fr^{-\frac{1}{2}}$, would be equivalent to the expression: $f \propto D^{-\frac{1}{2}}$.

A buoyancy induced instability has also been observed in isothermal helium plumes as indicated in Fig. 1 [28]. The Strouhal number of the non-reacting flow is well correlated by the inverse Froude number, but yields a different power law exponent than the reacting flow case. This is not surprising considering that the local density gradients in the reacting and non-reacting structures are quite different. Although numerical simulations of the pulsation phenomena in buoyant plumes has been accomplished [35], the pulsing nature of buoyant fires remains to be modeled from detailed consideration of the conservation equations.

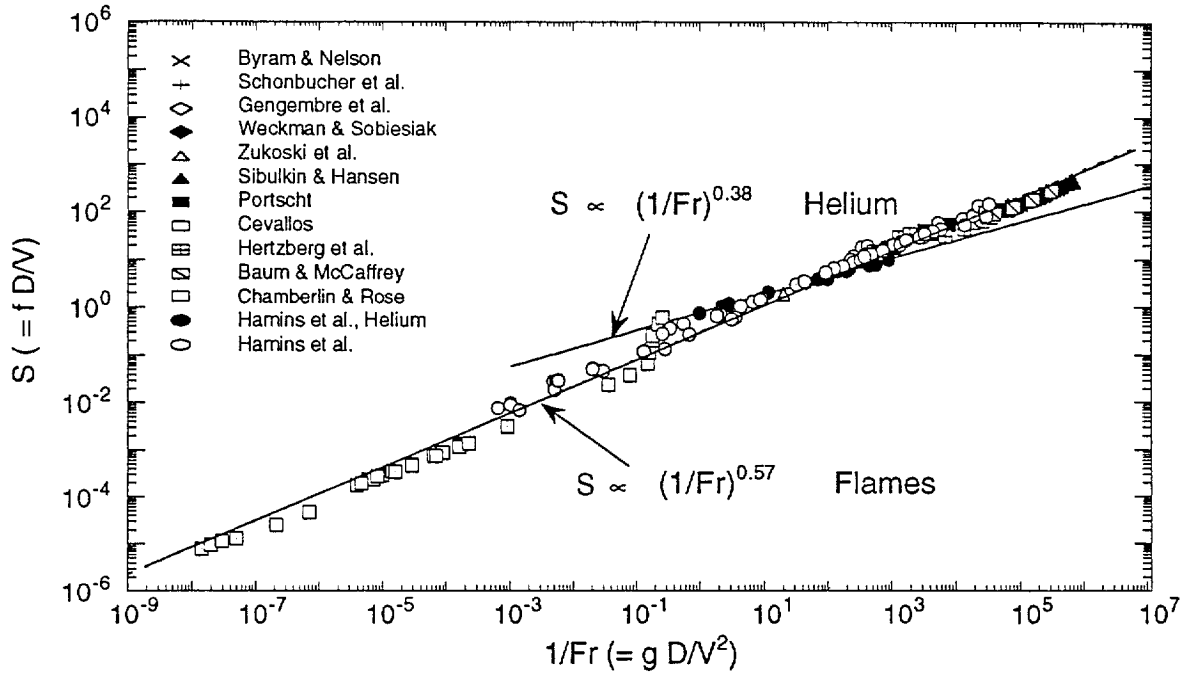

Figure 1 The Strouhal number as a function of the inverse Froude number for flames burning liquid, solid, and gaseous fuels and for a helium plume.

Flame Height

The shape and height of a fire have important implications in terms of fire hazard. In an enclosure, direct convective heat transfer to a ceiling may have dramatic consequences in terms of time to flashover. Flame height is also a key parameter in radiative heat transfer calculations to targets external to the fire and is related to possible ignition of a secondary object. In global burning rate models, the flame height impacts the calculated radiative feedback rate to the fuel surface and thereby influences predictions of fire growth and spread. In zone fire models, the calculation of flame height impacts estimates of radiative flame emission, the occurrence of reignition in upper layer gases in an enclosure, and estimates of the thermal insult on structural members [36]. McCaffrey [37] reviewed the large number of studies that have investigated flame heights, covering a wide range of burner diameters and different fuels. A common definition for flame height (or boundary) is that of the visible edge of flame luminescence. For turbulent diffusion flames, early research often relied on visual observation to estimate an average flame height. Zukoski et al. [17] used the 50% visible intermittency height to define a characteristic flame height (Z_f), which is defined as the location where the flame resides above and below this threshold 50% of the time.

The flame height correlations of Zukoski et al. [17] and Heskestad [38] are commonly used in the fire literature. Heskestad's algorithm relates flame height to a power law in terms of $N(\dot{Q})$, a non-dimensional heat release rate:

$$Z_f/D = -1.02 + 15.6 \cdot N(\dot{Q})^{0.2} \qquad (3)$$

TABLE 1--Thermochemical and combustion properties of several fluids.

Fuel	χ_s	T_b, K	H_c, MJ/kg	l_s, cm	r	χ_r
Methane	...	112	50.0	...[a]	12.9	0.21[b]
Propane	...	231	46.4	16	15.7	0.24[b]
Acetylene	...	...	48.2	1.9	13.3	0.28[b]
Methanol	0.063	338	20.0	...[a]	6.9	0.22
Ethanol	0.037	351	26.8	23	9.4	0.18
Acetone	0.020	329	28.6	21	9.9	0.27
Heptane	0.011	371	44.6	12	15.2	0.33
Toluene	0.013	383	40.5	0.6	13.5	0.34
PDMS[c] (D4)	0.017	449	24.8	0[d]	7.5	0.37
PDMS[c] (MD_2M)	0.016	467	28.8	0[d]	8.9	0.37
PDMS[c] ($MD_{15}M$)	0.13	≈648[e]	24.8	0[d]	7.5	0.31

a The smoke point has not been accurately measured, but is expected to be extremely large.
b χ_r is listed for large fuel flow rates, see Figs. 7 and 8 for χ_r as a function of mass flux in the 0.38 m burner.
c PDMS (polydimethylsiloxane) with $M=(CH_3)_3SiO$ and $D=(CH_3)_2SiO$.
d SiO_2, an oxidized particle, is a stable product that escapes the flame tip for all combustion conditions.
e Estimated temperature for thermal degradation (reversion) to volatile cyclics (D_3, D_4, ..., D_n).

where D is the pool diameter and $N(\dot{Q})$ is defined as:

$$N(\dot{Q}) = [c_p \cdot T_o/(H_c/r)]^3 \cdot (\dot{Q}_D^*)^2 \qquad (4)$$

r is the stoichiometric (mass based) ratio of air to fuel, c_p is the heat capacity of air at ambient temperature, T_o, and H_c is the heat of combustion for a particular fuel. $\dot{Q}_D^*$ is defined as:

$$\dot{Q}_D^* = \dot{Q}/(\rho_o \cdot c_p \cdot T_o \cdot (g \cdot D^5)^{0.5}) \qquad (5)$$

where ρ_o is the ambient air density and g is the gravitational acceleration. The parameter $N(\dot{Q})$ is proportional to the Froude number defined in Eq. 1 and is related to the fire heat release rate ($\dot{Q}$). The values of r and H_c can vary by a factor of two for different fuels as seen in Table 1.

Hasemi and Nishihata [39] studied small $\dot{Q}_D^*$ flames, where small $\dot{Q}_D^*$ was defined as $\dot{Q}_D^* < 0.1$, $N(\dot{Q}) < 10^{-5}$, or $Z_f/D < 0.5$. Intermediate and large flames are characterized by ($\dot{Q}_D^* > 0.1$). Hasemi and Nishihata [39] found that:

for small flames $\quad Z_f/D \propto (\dot{Q}_D^*)^2 \qquad (6a)$

for intermediate flames $\quad Z_f/D \propto (\dot{Q}_D^*)^{(2/3)} \qquad (6b)$

Zukoski et al. [17] correlated flame height to a power law in terms of $\dot{Q}_D^*$:

$$Z_f/D = 3.3 \cdot (\dot{Q}_D^*)^{(2/3)} \text{ for } \dot{Q}_D^* < 1 \qquad (7a)$$

$$Z_f/D = 3.3 \cdot (\dot{Q}_D^*)^{(2/5)} \text{ for } \dot{Q}_D^* \geq 1 \qquad (7b)$$

Zukoski et al.'s [17] algorithm can be related to the Heskestad [38] expression through $\dot{Q}_D^*$. Heskestad's and Zukoski's correlations given in Eqs. 3 and 7 relate the normalized flame height (Z_f/D) to the total fire heat release ($\dot{Q}$).

Figure 2 shows our measurements [40] of the normalized flame height as a function of $N(\dot{Q})$ in gaseous pool fires burning acetylene, propane, and methane in 0.10, 0.38, and 1.0 m water-cooled sintered-metal and sand-filled burners. Like Zukoski et al. [17], the 50% intermittency visible flame height was used to define the characteristic flame height. The bars on some data points represent minimum and maximum observed non-dimensional flame heights which varied from approximately 0.7 to 3 times the average flame height. Measurement uncertainty is estimated to be approximately 10%, which is smaller than the symbol size representing the data in Fig. 2 [40]. Also shown are the correlations of Zukoski (for CH_4, C_3H_8, and C_2H_2) and Heskestad. The correlations of Heskestad and Zukoski behave very similarly for $N(\dot{Q}) > 4 \cdot 10^{-5}$. For $N(\dot{Q}) < 4 \cdot 10^{-5}$, the predictions are significantly different. Heskestad's [38] correlation appears to adequately represent the data in Fig. 2 except for the high C_2H_2 mass flows, where the flames are smoky and the combustion efficiency is small.

In the original development of a flame height model based on the Froude number, Heskestad [41] proposes that the non-dimensional flame height should be written in terms of N and the sensible heat loss from the flame ($\dot{Q}_c$) as:

$$Z_f/D = f(N/\dot{Q}_c) \qquad (8)$$

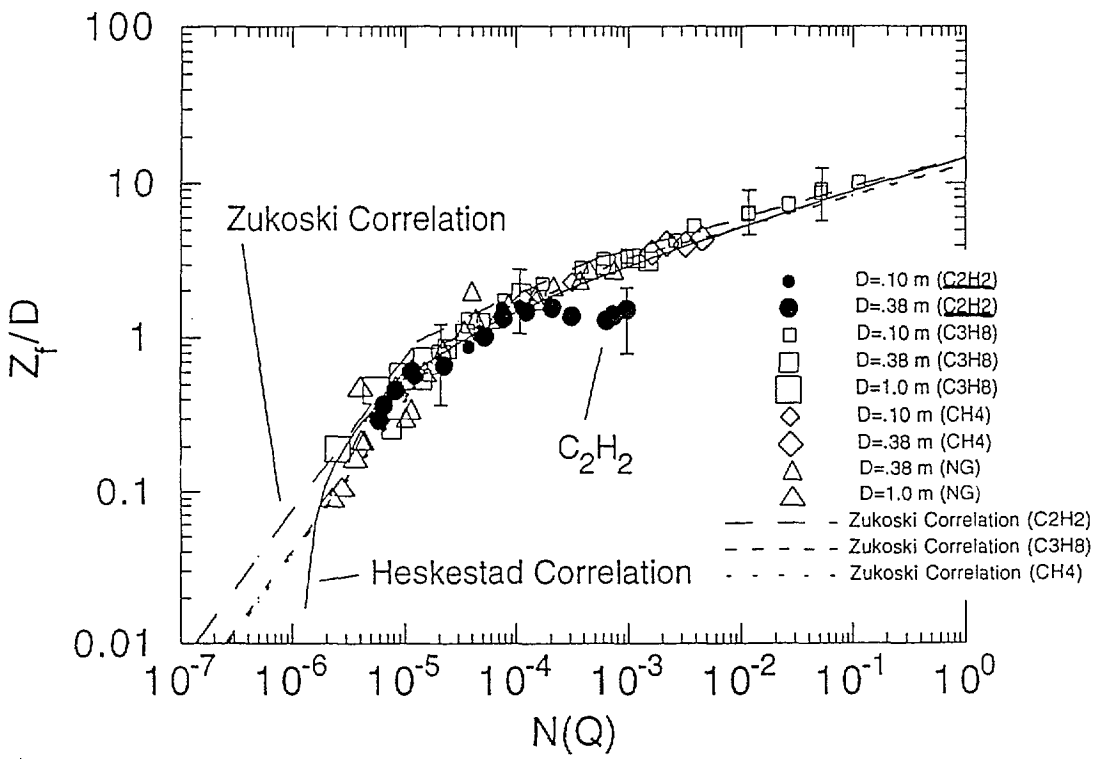

Figure 2 Measurements of the normalized flame height as a function of $N(\dot{Q})$. The flame height correlations of Heskestad [37] and Zukoski [17] are also shown.

where $N=N(\dot{Q}_c)$. Physically, $\dot{Q}_c$ is the flame enthalpy convected away by the plume to the surroundings. It is discussed in detail in Section 2.

Unfortunately, the fuels used to develop the flame height algorithms [17,38,39] relied almost exclusively on non-smoky fuels, where the non-dimensional parameter χ_c ($=\dot{Q}_c/\dot{Q}$) is typically greater than 0.7. Common fuels are often smoky and thus, it is of interest to test the flame height correlation for a fuel like acetylene, which has a high sooting tendency and which may have χ_c values much smaller than 0.7 [42]. An attempt to correlate the non-dimensional flame height according to Eq. 8 also failed to collapse the high mass flow acetylene results. This may be because the physics controlling the length scales in very sooty fires may be different than in non-smoky fires [43].

A fit of the same normalized flame height data used in Fig. 2 as a function of $\dot{Q}_D^*(\dot{Q}_c)$ fares much better as shown in Fig. 3. The correlation by Zukoski for $\dot{Q}_D^*(\dot{Q})$ is also shown, but as expected it does not correlate the data. These results imply that non-smoky fuels are reasonably predicted by the literature flame height correlations. For smoky fuels, however, the literature correlations do not do a good job of predicting average flame heights. A better fit is obtained when $\dot{Q}_c$, the sensible heat loss from a flame is considered. However, in most common fire scenarios, measurement of $\dot{Q}_c$ is impractical.

The Detailed Structure of Pool Flames

The turbulent nature of a fire plays an important role in mediating flame radiation. Local radiative emission is governed by the time-

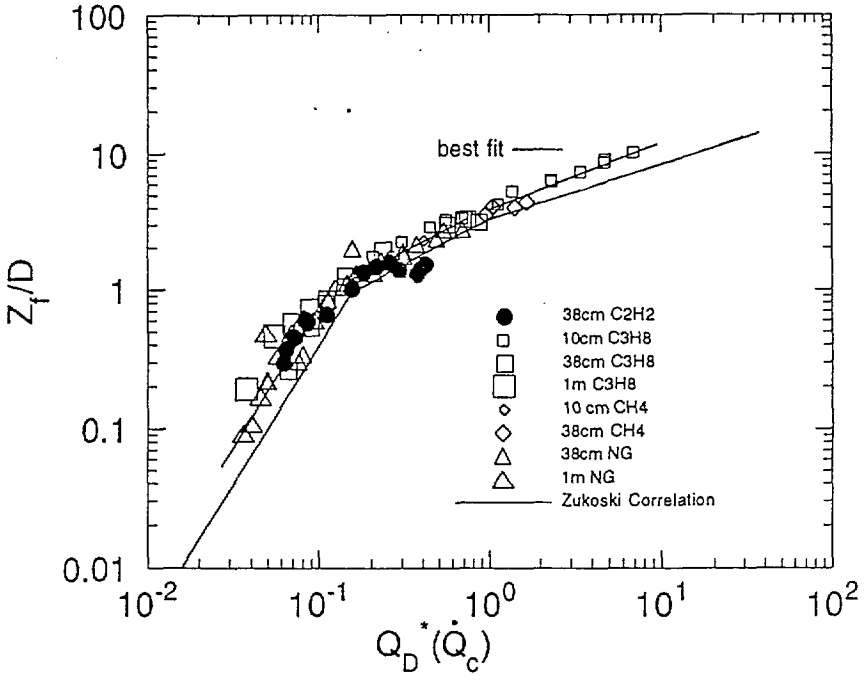

Figure 3 The measured flame height as a function of $\dot{Q}_D^*(\dot{Q}_c)$. Zukoski's correlation for $\dot{Q}_D^*(\dot{Q})$ is also shown.

varying correlated distributions of temperature and soot volume fraction. Because of the highly non-linear dependence of Plank's function, small uncertainties in flame temperature can propagate large errors in the calculation of radiative emission from a flame. In addition to particle radiation, emission by water and carbon dioxide must also be considered. Thus, it is of interest to understand the temporal and spatial structure of a turbulent fire. The structure of a steady laminar diffusion flame is defined by the scalar distributions of temperature and chemical species, including both soot particles and stable and unstable reactive radical gas phase species, and by the vector velocity field.

A complete set of flame structure information can be used to make calculations of radiative flame emission and feedback to the fuel surface, as well as estimates of the key chemical heat release pathways [44,45]. The structure of an unsteady turbulent fire is complicated by the time varying distributions of these quantities. The number of investigations on the detailed structure of buoyant turbulent pool fires is much, much smaller than in laminar flames. Enough information does exist in pool fires, however, to qualitatively understand trends in the mean temperature, velocity, and stable species concentrations [4,9,14,16,46-49].

McCaffrey [50] represented the mean temperatures and velocities as functions of the heat release. The mean centerline temperature rapidly increases from the fuel surface to a peak value of nearly 1200 K in a distance of approximately one pool diameter for buoyant 0.3 m propane pool fires [9]. Above the temperature maximum, the mean centerline temperature slowly decreases due to cooling by entrained air and a halt to the chemical reactions. In the intermittent zone, the mean temperature decreases, whereas in the persistent region, the temperature is essentially unchanging. In the intermittent region, McCaffrey [50] showed that the radial dependence of the mean axial temperature and velocity scaled like a gaussian function. The RMS temperature variation at a single location near the edge of a hydrocarbon fire is typically as large as 500 K, almost as large as the mean temperature itself [51].

The mean axial velocity profile also scales with the heat release [50]. At the pool surface, the gas phase fuel velocity is small for liquid fuels ($\approx$0.1 m/s) and even smaller for burning solids. Gas velocity in a fire rapidly accelerates above the pool surface, driven by the volume expansion associated with chemical reaction. A few centimeters above the pool surface, vertical speeds on the order of 1 m/s are obtained for buoyant 0.3 m propane pool fires [9]. The gas velocity continues to increase until the heat release stops near the top of the visible flame, with vertical speeds reaching 3 to 4 m/s at 0.2 to 0.4 m above the fuel surface [9]. The rms velocity variation has not been as carefully characterized.

The average of the time varying species concentration field in a turbulent flame bears some resemblance to that of a laminar flame. In laminar non-premixed flames, it has been shown that the temperature and many of the major and minor species concentrations are related through simple state relationships, which is a function of the local equivalence ratio [51,52]. Soot volume fraction does not correlate in this same manner. On the flame axis, the concentration of fuel decreases rapidly and the concentration of oxygen increases. In a turbulent flame, the time-averaged species concentration and temperatures are smoothed out. In most flame regions, their values do not obtain peak values as large as in laminar flames [4,9,14,16,46,49]. The concentration of intermediate species such as carbon monoxide, molecular hydrogen and the soot volume fraction do increase with distance above the fuel surface [9].

ENTHALPY BALANCE IN THE FLAME

There are wide differences in the radiative emission characteristics of

fires depending on the fuel composition. Flames burning methyl alcohol, for example, do not contain soot particles and appear blue in color due to non-equilibrium thermal processes. Flames burning H_2 are not visible at all. In contrast, hydrocarbon fires are extremely luminous due to significant concentrations of soot particles which emit blackbody radiation. Gas species such as carbon dioxide, water, and to a lesser extent carbon monoxide and hydrocarbon intermediates, emit infrared radiation in hydrocarbon and non-hydrocarbon fires, but the visible radiation intensity emitted by soot typically far exceeds that of gaseous emission. For some fuels, as the fire source becomes large, the rate of soot production exceeds the rate of soot oxidation and carbonaceous soot particles are convected through the fire to the surroundings. If the soot yield is very high, then flame radiation will be blocked and the fractional radiative emission will decrease.

Beyond spectral differences, radiated power differs with fuel type even for the same values of heat release, $\dot{Q}$. This implies that the simple assumptions of Froude modeling must be modified to account for differences associated with chemical influences on the structure of a fire.

The energy radiated from a flame is a key parameter in fire safety considerations. The magnitude of the radiative transfer to targets external to the flame affects the hazard posed by a particular fire and influences fire spread rates. Radiative transfer from the flame to the fuel surface is the dominant heat feedback mechanism in large fires, controlling the fuel mass evaporation rate.

An overall enthalpy balance about a diffusion flame shows that the actual heat release from chemical reactions ($\dot{Q}_a$) is equal to the sum of the energy convected from the buoyant plume to the surroundings ($\dot{Q}_c$), enthalpy feedback to the fuel surface ($\dot{Q}_s$), and energy radiated to the surroundings by high temperature soot particles and gas species ($\dot{Q}_r$):

$$\dot{Q}_a = \chi_a \cdot \dot{Q} = \dot{Q}_r + \dot{Q}_c + \dot{Q}_s \qquad (9)$$

where the actual heat release ($\dot{Q}_a$) is equal to the idealized heat release ($\dot{Q}$) modified by the combustion efficiency (χ_a). The idealized heat release ($\dot{Q}$) is defined as:

$$\dot{Q} = \dot{m} \cdot H_c \qquad (10)$$

where $\dot{m}$ is the mass vaporization rate (kg/s) and H_c is the heat of combustion (MJ/kg). Dividing through by $\dot{Q}$, Eq. 9 can be rewritten as:

$$\chi_a = \chi_r + \chi_c + \chi_s \qquad (11)$$

where χ_s is defined as:

$$\chi_s = \dot{Q}_s/\dot{Q} \qquad (12)$$

and represents the heat feedback to the fuel surface via radiation, convection and conduction. The fractional amount of total combustion enthalpy lost as sensible heat is defined as the convective heat loss fraction (χ_c):

$$\chi_c = \dot{Q}_c/\dot{Q} \qquad (13)$$

The fractional amount of total combustion enthalpy emitted from a flame is defined as the radiative heat loss fraction (χ_r):

$$\chi_r = \dot{Q}_r/\dot{Q} \qquad (14)$$

Radiative Emission

Figure 4 is a schematic drawing of the technique used to determine the

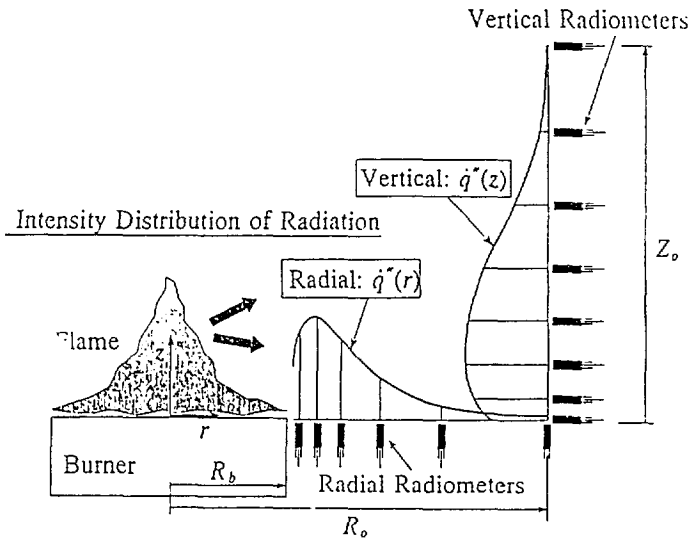

Figure 4 Schematic drawing of the methodlology to measure the radiative flux distribution over a surface surrounding the flame.

radiative flux distribution over a surface surrounding the flame. The radiated power ($\dot{Q}_r$) is determined by integrating the measured spatial distribution of radiant flux. At the same time, $\dot{Q}$ can be determined by monitoring the burning rate ($\dot{m}$). Figure 4 is a schematic of the location and orientation used to measure the radiated power from a flame. Typical profiles of the near field time-averaged radiative flux as a function of location in the radial and vertical directions are also shown. The radiative flux drops off very quickly in the radial direction, whereas in the vertical direction, the flux peaks at a vertical location equal to approximately 50% of the characteristic flame height. The vertical and radial flux distributions are numerically

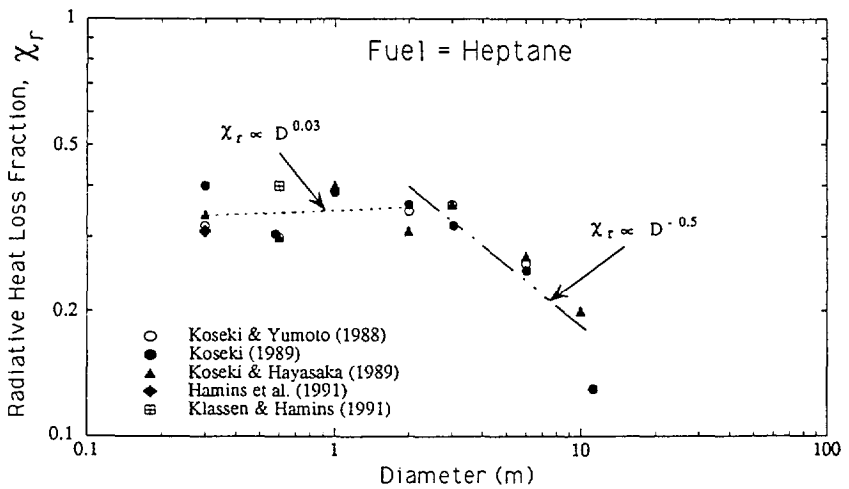

Figure 5 Measurement of χ_r as a function of pool diameter for heptane fires.

integrated to obtain the total radiant power output of the flame using the following expression:

$$\dot{Q}_r = 2\pi\left(\int r \cdot q''(r) \cdot dr + R_o \int z \cdot q''(z) \cdot dz\right) \quad (15)$$

where the symbols for the r axis, z axis, and R_o are defined in Fig. 4. This method has been used by a number of investigators. Jeng and Faeth [54] used this technique for methane jet flames. Subsequently, Gore [55] applied this technique to jet diffusion flames burning a variety of fuels. Hamins et al. [56] have determined χ_r from detailed radiant flux measurements for a number of different fuels and pool diameters.

Figure 5 shows measurements from several authors of χ_r as a function of pool diameter for fires burning heptane [56-60]. Two distinct regimes are delineated in the figure. For 0.1 m< D < 2 m, χ_r is relatively constant, whereas for D > 2 m, $\chi_r \propto D^{-\frac{1}{2}}$. Data for kerosene shows very similar dependencies [61].

Since measurements of the distribution of the radiant flux over a surface bounding the source is tedious and at times impractical, many measurements of radiative heat loss fraction reported in the literature rely on single point radiant flux data and the assumption of isotropy. For a spherical source, the total radiative power output $\dot{Q}_r$ (kW) is the product of the flux, q"(r), and the spherical surface area ($4\pi r^2$):

$$\dot{Q}_r = 4\pi r^2 \cdot q''(r) \quad (16)$$

where R is the sphere radius. The incident thermal radiation flux (q") is proportional to the inverse square of the distance from the source. McCaffrey [62] used single location measurements and the assumption of radiative isotropy to evaluate χ_r for medium sized pool fires. Modak [63] and Bouhafid et al. [3] measured radiative flux at various distances from pool fires. Modak [63] concludes that the assumption of an equivalent isotropic emitter improves with distance from the fire and is approximately valid for distances from the pool center equal to ten diameters.

Figure 6 shows our measurements of the power radiated to the surroundings ($\dot{Q}_r$) as a function of diameter for burning pools of a number of hydrocarbon and polydimethylsiloxanes (siloxane) fluids (Buch et al., 1995). $\dot{Q}_r$ is related to χ_r through Eq. 14 and to $\dot{m}$ through Eq. 10, yielding:

$$\dot{Q}_r = \dot{m} \cdot H_c \cdot \chi_r \quad (17)$$

As shown in Fig. 5 for heptane, $\chi_r \approx$ constant for D < 2 m, leading to the result that the radiated power is proportional to the burning rate (i.e., $\dot{Q}_r \propto \dot{m}$ for D < 2 m). Figure 6 shows that for the same pool diameter, $\dot{Q}_r$ differs by an order of magnitude between fuels and is largest for the hydrocarbons (heptane and toluene) and oligomeric short chain siloxanes (MM, MDM, MD2M, and D4) and is more than an order of magnitude smaller for alcohols or polymeric siloxanes ($MD_{15}M$ and $MD_{58}M$) [64]. The notation describing the chemical structure of the siloxanes is explained in Table 1.

For D > 2 m, the mass vaporization flux ($\dot{m}$") is approximately constant [65], and therefore, $\dot{m} \propto D^2$. For heptane and kerosene, $\chi_r \propto D^{-\frac{1}{2}}$ (see Fig. 5). This leads to an expression that can be expected for typical liquid hydrocarbons (i.e., $\dot{Q}_r \propto D^{1.5}$). Mudan and Croce [66] show measurements of the emissive power for liquified natural gas (LNG) which suggest that $\dot{Q}_r \propto D^2$ for D >>2. This implies that $\chi_r \approx$ constant for D >> 2 m for LNG, quite different from the results seen in Fig. 5 for a larger hydrocarbon like heptane, which has a higher sooting tendency.

Table 1 lists χ_r for a number of fluids burning in a 0.3 m diameter pool. Table 1 shows that the fluid type has a significant influence on χ_r, which is smallest for the non-luminous methanol fires.

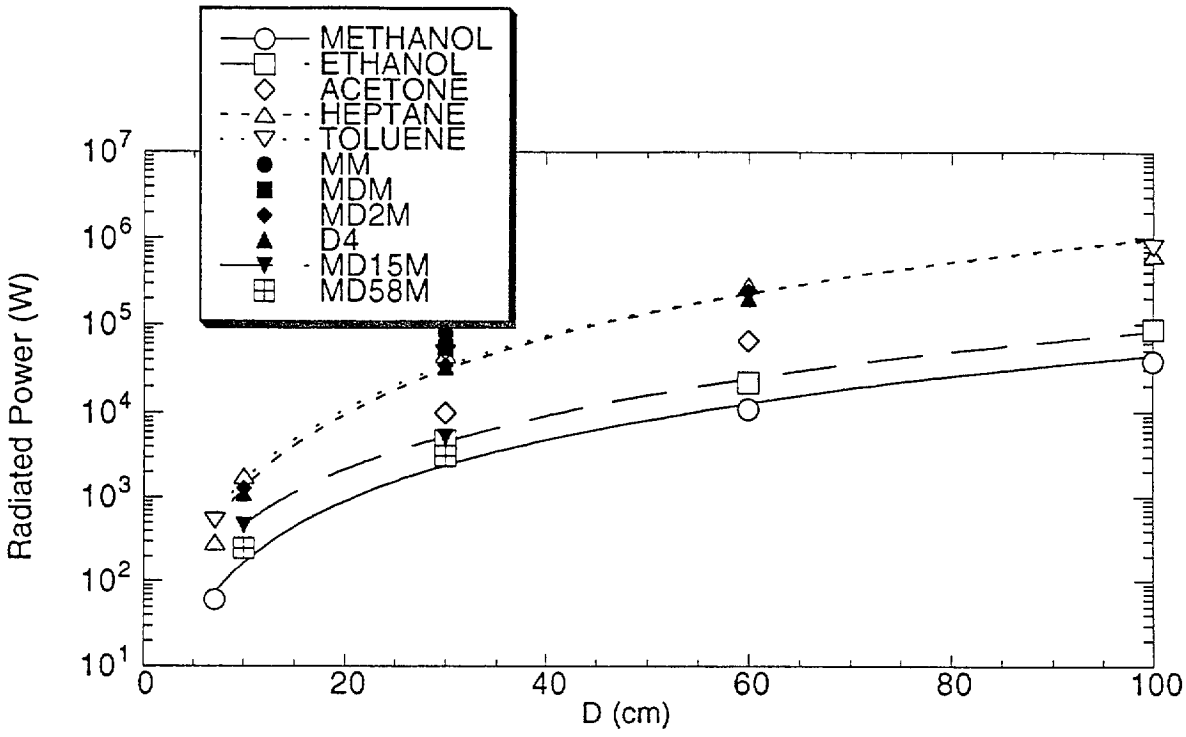

Figure 6 Measurement of $\dot{Q}_r$ as a function of pool diameter for fires burning a number of liquid fuels.

As $\dot{Q}_r$ increases, $\dot{Q}_s$, the heat feedback rate to the pool surface can also be expected to increase. Other factors, however, such as radiation blockage by fuel vapor, pyrolysis intermediates, and soot particles, play an important role in mediating radiative heat feedback [67,68]. Thus, the modeling of $\dot{Q}_s$ requires a detailed understanding of flame structure, and cannot be predicted from global flame energetics alone. Detailed measurements of $\dot{Q}_s$ on the pool surface could also differentiate the relative importance of radiative and convective transfer in intermediate sized pool fires. For large burner diameters (D >2 m), radiative transfer is expected to dominate.

For a hydrocarbon fire, the ratio ($\dot{Q}_c/\dot{Q}=\chi_c$) typically takes on values much less than unity [42], depending on a number of factors including, most importantly, the fuel type and fire size which controls χ_a and χ_r. Expe imentally, the sensible enthalpy loss from a fire ($\dot{Q}_c$) can be estimated from the heat carried by the combustion products [69]. In an exhaust duct, the sensible enthalpy loss from the fire can be expressed as [40]:

$$\dot{Q}_c = V_a \cdot A \cdot \rho \cdot c_p \cdot \Delta T \qquad (18)$$

where V_a is the velocity of the exhaust at the location of the thermocouple array, A is the duct area, ρ is the gas density, c_p is the heat capacity of the exhaust gases, and ΔT is the temperature difference between ambient and the average exhaust temperature, measured by thermocouples.

Measurements of $\dot{Q}_c$, $\dot{Q}_r$, $\dot{Q}_s$, and $\dot{m}$ for a particular fuel allow determination of χ_a from Eqs. 9 and 10. Experimentally, enthalpy losses to a water cooled burner ($\dot{Q}_s$) can be determined by monitoring the volumetric flow of cooling water and the temperature increase of the water [40]. Alternatively, χ_a can also be determined by oxygen

depletion calorimetry [42]. Tewarson [42] related the smoke point height (l_s) to global combustion properties such as χ_r, χ_a, and χ_c from calorimetry and radiative flux measurements made on a large number of solid, liquid, and gaseous fuels burning in small diameter pools. Table 1 lists the smoke point height (l_s) for several fuels. l_s is defined as the critical flame length at which soot escapes from the flame tip [70]. Typical hydrocarbons are characterized by l_s values ranging from 0.5 to 20 cm. Small values of l_s, are associated with hydrocarbons with a higher tendency to soot. Methanol flames contain near-zero concentrations of soot and thus are characterized by infinite smoke point heights. Although l_s is helpful in ranking the combustion efficiency of various organic fuels, combustion efficiency is also a function of the fuel flux. This is seen in Fig. 7, where the measured values of χ_r, χ_s, and χ_c and the calculated values of χ_a are presented as a function of the mass burning flux of acetylene in a 0.38 m diameter water-cooled sintered-metal burner. The enthalpy feedback to the burner (χ_s defined in Eq. 12) is relatively small except for small fuel fluxes. The enthalpy feedback decreased with increased fuel flux, consistent with thin film models of convective transfer [6,7]. As the acetylene mass vaporization flux ($\dot{m}''$) increased, χ_r increased and χ_c decreased. For very small acetylene mass fluxes, the flames were non-smoking and χ_a was determined to be close to unity. This is because hydrocarbon fuels like acetylene with a high tendency to soot, typically yield smoke only for moderate and high mass fluxes. As the acetylene mass flux increased, Fig. 7 shows that the fires produced copious quantities of soot and χ_a decreased, obtaining values as low as 0.6. For small mass fluxes, χ_c took on values nearly 0.4.

Similar measurements for methane (and natural gas composed of ≈96%

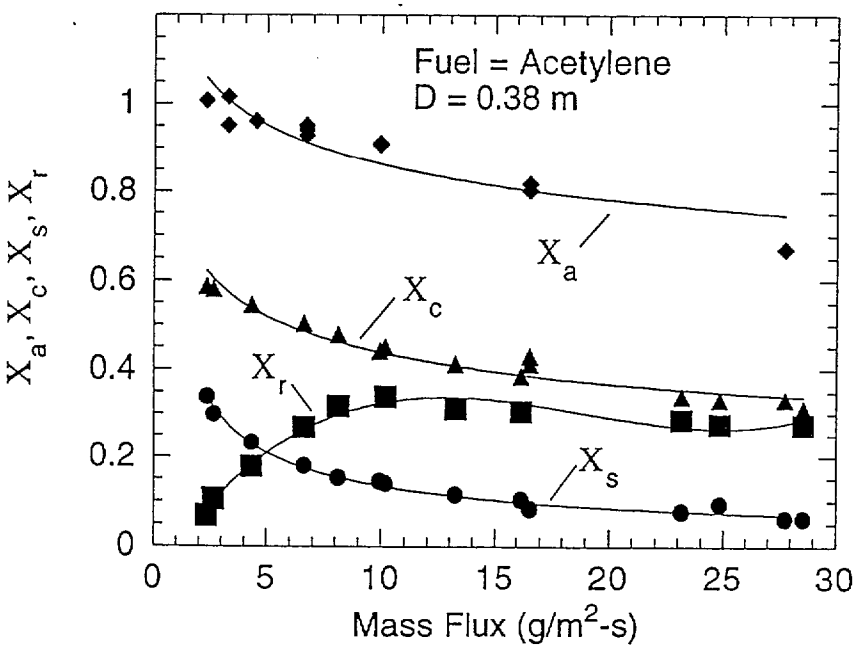

Figure 7 Measurements of χ_r, χ_s, and χ_c as a function of the mass burning flux of acetylene in a 0.38 m burner. The calculated value of χ_a is also shown.

methane) are shown in Fig. 8. Because these fires were not observed to produce smoke, it was assumed that $\chi_a \approx 1$. A comparison of Figs. 7 and 8 shows that for the same mass flux, the χ_r values for natural gas and methane were smaller and the χ_c values were generally larger than in the acetylene flames.

ENTHALPY BALANCE AT THE FUEL SURFACE

The heat feedback rate, $\dot{Q}_s$ (kW), from the flame to the pool surface can be partitioned into the three major heat transfer mechanisms: conduction [71], convection [72-74] and radiation [75-79]. A large number of studies have investigated each of these mechanisms in an effort to accurately model mass vaporization rates in burning pools. The relative contributions of each of these are related to geometrical parameters such as the pool diameter, burner material, and lip height, but more fundamentally to the structure of the flame itself, including the flame shape and the spatial distribution of temperature, species concentration and soot volume fraction.

Hottel [75] represented heat transfer to the pool surface in terms of global flame properties:

$$\dot{Q}_{s,cond} = k'\pi D(T_f - T_s) \quad (19)$$

$$\dot{Q}_{s,conv} = hA_s(T_f - T_s) \quad (20)$$

$$\dot{Q}_{s,rad} = \sigma V A_s(T_f^4 - T_s^4)(1-\exp(-\Gamma \cdot D)) \quad (21)$$

where $\dot{Q}_{s,cond}$, $\dot{Q}_{s,conv}$, and $\dot{Q}_{s,rad}$ are respectively conduction, convection and absorbed radiation heat transfer to the pool surface, k' (kW/m·K) is a conduction coefficient, D (m) is the pool diameter, A_s (m^2) is the pool surface area, T_f (K) is the flame temperature, T_s (K) is the pool surface temperature, h ($kW/m^2 \cdot K$) is a convective heat transfer coefficient, σ is the Stefan-Boltzmann constant, V is a dimensionless flame-pool surface radiative configuration factor, and Γ (m^{-1}) is a radiative extinction coefficient.

Hottel [75] noted that when D is small ($D \ll 1$), conduction dominates the heat feedback because convection and radiation are proportional to D^2 and conduction is proportional to D. When D is large, the importance of conduction diminishes and radiation eventually dominates convection. This is because $\Gamma \cdot D$ in Eq. 21 becomes large and radiation is proportional to T_f^4. Burgess and Hertzberg [76], using Hottel's [75] bulk properties formulation for pool burning and Blinov and Khudyakov's [80] burning rate data, determined that radiative transfer becomes dominant over convection for pool diameters from 0.1 to 0.5 m depending on fuel type. Below these sizes, convection was found to be important.

A schematic diagram of the enthalpy balance in a liquid pool fire is shown in Fig. 9 for a quasi-steady state system [81]. Such a system is achieved by adding fuel from a reservoir into the pool bottom at a rate that matches the fuel burning rate, such that the fuel level remains constant. The gradual growth of the thermal layer inside the liquid pool ($\dot{Q}_{corr}$) must also be considered. A short time after ignition, the mass vaporization rate ($\dot{m}$) in such a system is nearly constant, but the bulk temperature throughout the pool continues to gradually increase [81], which represents a flame enthalpy loss mechanism ($\dot{Q}_{corr}$). The enthalpy balance for a control volume about the liquid pool can be represented as:

$$\dot{Q}_s = \dot{Q}_{s,cond} + \dot{Q}_{s,conv} + \dot{Q}_{s,rad} - \dot{Q}_{reflect} \quad (22)$$

$$\dot{Q}_s = \dot{m} \cdot H_g + \dot{Q}_{rerad} + \dot{Q}_{loss} + \dot{Q}_{corr} \quad (23)$$

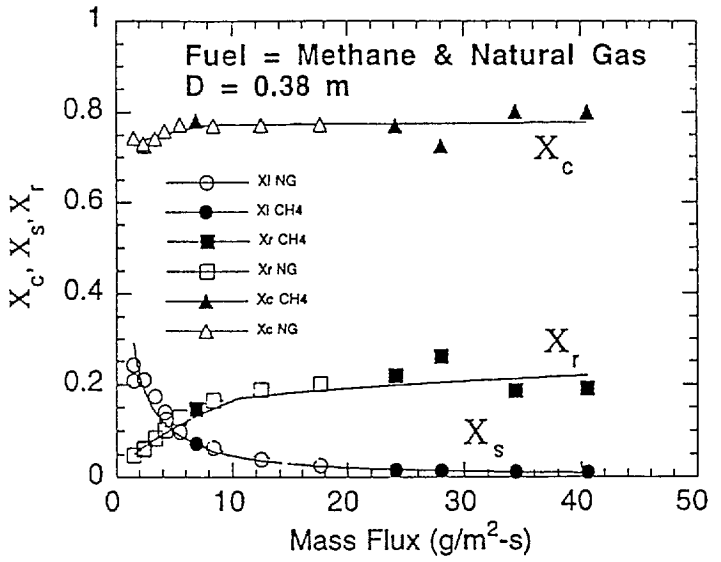

Figure 8 Measurements of χ_r and χ_s as a function of the mass burning flux of methane and natural gas in a 0.38 m burner. The calculated values of χ_c are also shown.

The net rate of heat feedback to the pool surface, $\dot{Q}_s$ (kW), is determined by the sum of the rates of convective ($\dot{Q}_{s,conv}$), conductive ($\dot{Q}_{s,cond}$) and radiative ($\dot{Q}_{s,rad}$) feedback. The rate of absorbed radiative enthalpy is equal to the incident ($\dot{Q}_{s,rad}$) minus the reflected rate of radiative enthalpy ($\dot{Q}_{reflect}$). The amount of surface reflection ($\dot{Q}_{reflect}$) depends on the angle of incident radiation and the refractive index of the fuel [81], where H_g (kJ/kg), for a steadily burning fire, is an effective heat of gasification defined as:

$$H_g = H_v + \int C_p \cdot dT \qquad (24)$$

H_v (kJ/kg) is the latent heat of vaporization at the pool surface temperature, C_p (kJ/kg·K) is the specific heat of the liquid fuel and the limits of integration are from ambient temperature (T_o) to the pool surface temperature (T_s). These terms are balanced primarily by the product: ($\dot{m} \cdot H_g$).

The width of the arrows in Fig. 9 symbolize the approximate importance of each of the key terms in the enthalpy balance occurring in a 0.30 m heptane pool fire. A detailed heat balance must consider other thermal sources and sinks. These include heat gain due to conduction through the metal burner walls, heat losses due to radiation from the fuel surface to the surroundings ($\dot{Q}_{rerad}$), losses from the bottom and sides of the burner ($\dot{Q}_{loss}$). The loss terms ($\dot{Q}_{rerad}$ and $\dot{Q}_{loss}$) act to diminish the fraction of enthalpy available for fuel vaporization, but are typically small when compared to the term ($\dot{m} \cdot H_g$) for liquid fuels. The combustion of a solid material can have a high surface temperature, leading to large values of $\dot{Q}_{rerad}$. Another possible contribution to the overall heat balance is from water condensation ($\dot{Q}_{water}$) on the fuel surface. Condensation of gas-phase water molecules, diffusing from the flame towards the relatively cool fuel surface, can impact the fuel burning rate measurement and increase the enthalpy of the pool. The impact of this process may be non-trivial for fuels with pool surface temperatures significantly less than the water boiling point (T_s<<373K).

Experimental characterization of the local heat transfer to the pool surface is essential for the development and validation of detailed models which predict the burning rates of liquid hydrocarbons and solid

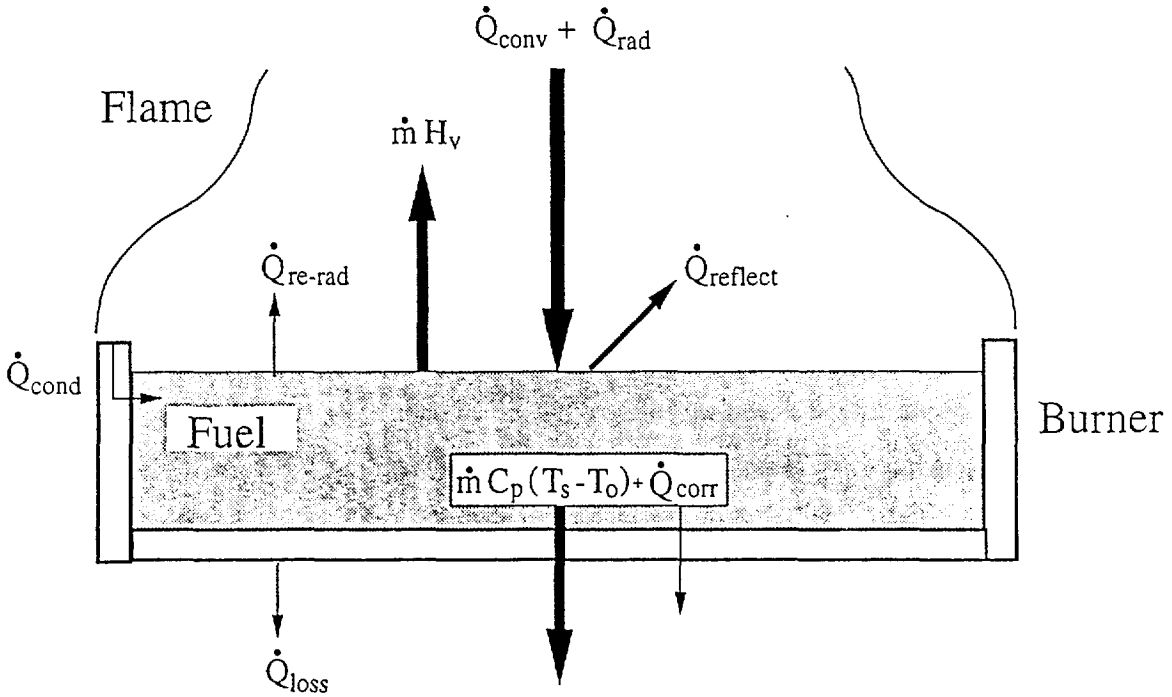

Figure 9 Schematic drawing of the enthaply balance for a pool fire burning a liquid fuel.

polymers. Yet, only a limited number of experiments have measured local heat transfer to the fuel surface.

Previous measurements of the local radiative or net heat flux at the surface of pool fires are listed in Table 2. Measurements have been conducted on pools varying in diameter (D) from approximately 0.01 to 3 m for a number of different liquid fuels and for solids including polymethylmethacrylate (PMMA). Studies of local mass vaporization rates have been conducted using ring pool burners [2,81,82] and insulated fuel wells [83] where local measurement of $\dot{m}$ in conjunction with Eq. 23 allows estimate of the local heat flux.

In their extensive investigation of pool fires, Blinov and Khudyakov [2] measured the burning rate of numerous hydrocarbon fuels in different sized concentric ring burners including a 0.80 m four-ring burner and a 0.30 m four-ring burner. Fuels tested included benzene, gasoline, kerosene and diesel oil. For all fuels, the burning rates were highest in the center ring, decreased away from the center and increased in the outer ring. These results were qualitatively different from the measurements reported by Akita and Yumoto [82] for methanol. Hamins et al. [81] measured burning rates in a 0.30 m four-ring burner and found that the mass vaporization flux ($\dot{m}''$) was nearly constant (within 20%) as a function of ring location on the pool surface for both luminous and non-luminous fuels.

In a series of square pool fires burning polymethylmethacrylate (PMMA), Modak and Croce [84] measured a monotonic decrease in burning rate from pool center to pool edge. For a PMMA square (0.31 m x 0.31 m), the local burning rate at the pool edge was approximately half the burning rate at the pool center.

TABLE 2--Heat feedback measurements in pool fires.

Reference	Fuel	D, m	$\dot{Q}''_{rad}$	$\dot{Q}''_{net}$	Steady State?	Comments
Blinov & Khudyakov (1961)	benzene gasoline kerosene oil	0.03-.8		X	yes	ring burner
Corlett & Fu (1966)	methanol acetone	0.006-0.3	X		yes	insulated fuel well
Akita & Yumoto (1965)	methanol	0.1-0.3	X		yes	ring burner
Yumoto (1971)	gasoline hexane	0.6-3	X	X	yes	pool center
Modak & Croce (1977)	PMMA	0.2		X	no	recession rate
Alger et al. (1979)	methanol JP-5	3	X		no	Gardon gauges
Shinotake et al. (1985)	heptane	0.3-1.0	x	x	no	dual Gardon gauges
Hamins et al. (1994)	methanol heptane toluene MMA	0.3	X	X	yes	ring burner/ radiometer

Local radiative heat fluxes have been measured using dual Gardon gauges [85,86], aspirated radiometers [87] or a windowless, nitrogen purged, water-cooled narrow view-angle detector [81]. Yumoto [85] measured heat feedback to intermediate-sized ($0.6\ m < D < 3.0\ m$) gasoline and hexane pool fires using dual Gardon gauges with different emissivities, but measurements were made at the pool center only. Alger et al. [87] measured the radiative feedback to large scale (3 m) methyl alcohol pool fires using Gardon and transpiration radiometers at several pool locations. They found that the radiation decreased from the pool center towards the pool edge by almost a factor of two, consistent with the results of Modak and Croce [84]. Shinotake et al. [86] determined convective and radiative heat feedback near the center of intermediate sized pools burning heptane by use of dual Gardon gauges with different surface emissivities. Their results showed that nearly 65% of the heat feedback near the pool center was due to radiation in a 0.3 m heptane fire. In those experiments, however, a thin fuel layer was floated over water, and the fuel was not maintained at a constant level. Corlett and Fu [83] estimated the local radiative heat transfer at several locations on the surface of methyl alcohol and acetone pool fires ($0.05m< D <0.225m$) using a small insulated well filled with fuel, but only a few measurements near the pool center were conducted.

Hamins et al. [81] characterized systematically the heat feedback rate to the surface of 0.30 m pool fires. The radial variation of both the mass vaporization rate and the incident radiative heat flux were measured. Figure 10 shows the absorbed radiative heat flux ($\dot{Q}''_{r,abs}$) normalized by the local net heat flux ($\dot{Q}''$) as a function of location on the surface of 0.30 m pool fires burning toluene, heptane and methyl

alcohol. The absorbed radiative flux is the difference between the incident and reflected fluxes. The percentage of absorbed radiative heat feedback integrated over the pool surface was largest for toluene, followed by heptane and methanol as indicated in the figure. In Fig. 10, the difference from a value of 1.0 can be attributed to convection (see Eq. 20). Radiation was found to play an important, if not dominant role, in the heat feedback to 0.30 m pool fires for both luminous and non-luminous flames.

These results imply that the burning rate of luminous pool fires (0.3 m < D < 1 m) may be adequately modeled by a detailed analysis of the local radiative heat transfer at the pool center or any other location on the fuel surface. In such models, neglecting convective heat transfer would introduce some small error (<20%) in the prediction of the fuel burning rate. This error would diminish for large diameter pools (D>1 m), as radiative heat transfer becomes relatively more important.

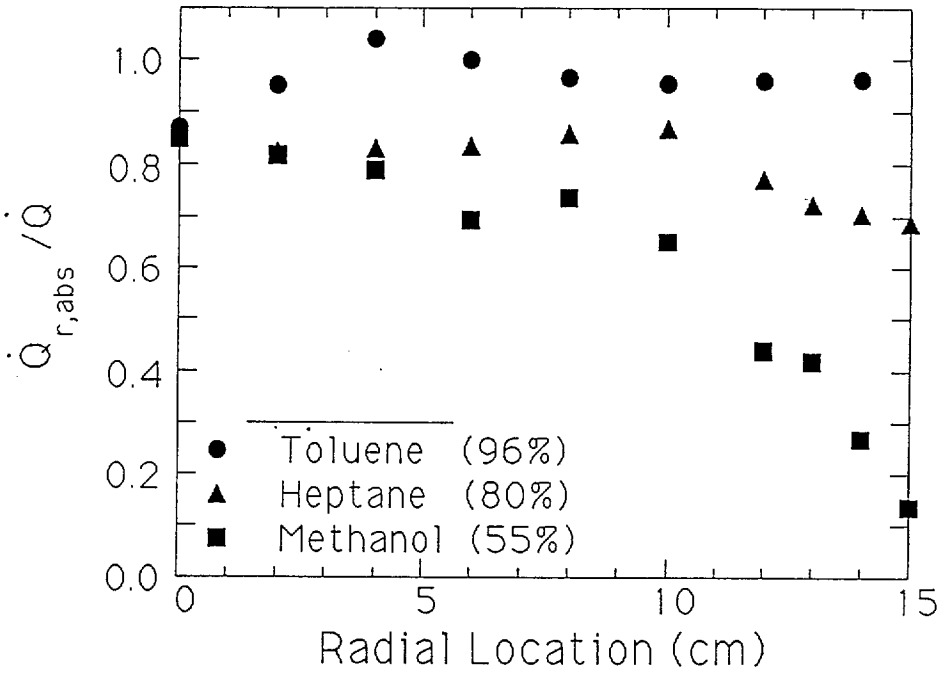

Figure 10 The normalized absorbed radiative heat flux as a function of location on the surface of 0.30 m pool fires. Numbers in parenthesis indicate the percentage of heat feedback due to radiation.

Mass Vaporization Rate

The heat flux to the surface of a pool fire and the mass flux vaporizing from the pool are coupled in a positive feedback loop. The rate of fuel evaporation depends on the rate of heat feedback from the flame to the fuel surface and the mass vaporization rate controls the total heat release rate and thereby the rate of heat feedback.

The steady mass vaporization rate is related to the ratio of heat transferred to the fuel surface ($\dot{Q}_s$) divided by the heat needed to

gasify the fuel (H_g). From Eq. 23 with $\dot{Q}_{rerad}$, $\dot{Q}_{loss}$, and $\dot{Q}_{corr}$ considered small compared to the enthalpy of gasification term ($\dot{m} \cdot H_g$):

$$\dot{m} \approx \dot{Q}_s / H_g \qquad (25)$$

Equation 25 assumes that heat losses to the burner, re-radiation by the fuel surface and other enthalpy loss terms are small. For a burning liquid pool in steady state, the surface temperature has been measured to be near the fuel boiling point [88]. For a solid fuel, the surface temperature is related to condensed phase degradation kinetics and is often called the pyrolysis temperature [89]. The total mass evaporation rate ($\dot{m}$) is determined by integrating over the pool surface:

$$\dot{m} = 2\pi \cdot \int \dot{m}''(r) \cdot r \cdot dr \qquad (26)$$

where $\dot{m}''(r)$ ($kg/m^2 \cdot s$) is the local mass vaporization rate of fuel. The average mass vaporization flux $\dot{m}''$ is related to the fuel burning rate (v), which is defined as:

$$v = \dot{m}'' / \rho_c \qquad (27)$$

and has units of length per unit time, where ρ_c is the density of the condensed phase fuel.

Using Eqs. 10 and 25, Eq. 12 can be expressed as the ratio of the heat of gasification, H_g (kJ/kg) to the ideal heat of combustion, H_c (kJ/kg):

$$\chi_s = H_g / H_c = \dot{Q}_s / \dot{Q} = 1/B \qquad (28)$$

χ_s in Eq. 28 is the reciprocal of the diffusive transfer number, the B number, as cited in the literature [76,90]. The value of χ_s is independent of the mass vaporization rate and depends mainly on intrinsic properties of the fuel. Table 1 shows that χ_s can vary by a factor of five or more among some common liquid fuels.

Compiling data for a very large number of fuels, Babrauskas [65] showed that the mass vaporization flux ($\dot{m}''$) obtains an asymptotic limit for large burner diameters. The pool diameter for which the limit was obtained, differed from fuel to fuel, but was typically on the order of

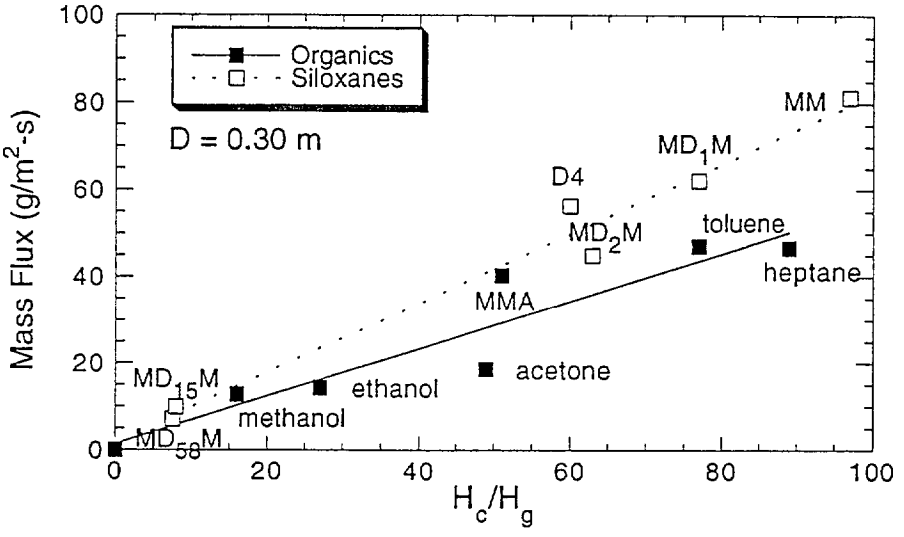

Figure 11 The measured fuel mass flux as a function of the fuel B number for a number of hydrocarbons and siloxanes burning in a 0.3 m burner.

a few meters for hydrocarbon fuels. Burgess and Hertzburg [76] showed that a plot of $\dot{m}''$ for hydrocarbons for large pool diameters was well correlated by the B number (χ_s^{-1}). It is of interest to consider the B number correlation in terms of (1) intermediate sized pool fires and (2) non-hydrocarbon fuels. Polydimethylsiloxanes (PDMS or siloxanes) are industrial fluids used in a wide range of applications. A combustion product of these fluids is SiO_2 particles which significantly impacts the radiation characteristics of the fires. Figure 11 shows the measured mass flux as a function of fuel B number ($= \chi_s^{-1}$) for a number of hydrocarbons and siloxanes burning in a 0.3 m pool [64]. Both, the siloxanes and the hydrocarbons are fairly well correlated by the B number. Figure 11 shows that the smaller oligomeric siloxane chains (MM, MD_1M, MD_2M and D4) burn much faster than the larger polymeric siloxanes ($MD_{15}M$ and $MD_{58}M$). In an analogous fashion, the hydrocarbons (heptane and toluene) burn faster than the alcohols. Plots similar to Fig. 11 can be constructed for burning hydrocarbons in a series of pool diameters. Figure 12 is a plot of the ratio of the fuel mass flux to the fuel B number ($\dot{m}''/B$) as a function of pool diameter for hydrocarbon fuels. A similar correlation could be developed for the siloxane fluids and plotted in Fig. 12. These results can be used to estimate the mass vaporization rate of typical hydrocarbon fuels for any burner diameter, assuming quiescent, freely burning conditions and that the fuel B number is known. Not surprisingly, the shape of the function in Fig. 12 is highly similar to the shape of a plot of the mass flux as a function of pool diameter for a fuel like toluene. Indeed, Fig. 12 is based on mass flux measurements for toluene and a number of other fuels. In addition, the correlation is limited to hydrocarbon fuels and will not predict mass evaporation rates for fuels with little tendency to form soot, such as the alcohols, methanol and ethanol. For these fuels $\dot{m}'' \approx$ constant, independent of pool diameter.

Vaporization Rate Models

Because of the complexities associated with heat and mass transfer, and gas phase kinetics in a turbulent fire, it is not currently possible to predict fuel vaporization rates from detailed solution of the conservation equations without resorting to empirical shortcuts. Thus, semi-empirical models of varying complexity have been developed, exploiting our knowledge of fluid dynamics, chemistry, and heat transfer in reacting systems. In general, the current models can be divided into global models and field models. Both types contain a large number of interacting submodels.

Global models often assign one or several zones of constant properties such as temperature or species concentrations. Transport is ignored. A mean beam length radiation submodel is often used to predict radiative transfer to the fuel surface [6,7,75]. The mean beam length is related to the flame shape. For small Froude numbers with a cylindrical flame shape, the mean beam length is related to the pool diameter and the flame height. Hayasaka and Koseki [91] used a mean beam length model with global flame properties and compared their predictions with measured burning rates for pools up to 10 m in diameter. Their model, however, has not been tested on fuels other than kerosene. Modak and Croce [84] calculated the radiative heat flux from the flame to a surface element on a burning pool (0.18 m) of PMMA in terms of an empirical time-averaged flame shape, an effective radiation temperature, and a mean gray-body absorption-emission coefficient. These parameters were all independently measured whereas convection was assumed to be negligible. Orloff and de Ris [6,7] represented the fire as a time averaged volume of constant property gases. Their measured radiative heat loss fraction (χ_r) was used to estimate a global absorption-emission coefficient. Measured flame shapes were used to calculate a mean beam length and convective heat feedback was estimated

from experiments on a water cooled gas burner. The flame temperature was taken as a constant for all fuel types. Model predictions were compared to measurements for pools burning liquid methanol and solid thermoplastics. Unfortunately, the efficacy of this particular approach depends on knowledge of χ_r which varies significantly as a function of pool diameter and mass flow rate, as seen in Figs. 5, 7, and 8. Global models are also sensitive to total heat release, which depends on the combustion efficiency, χ_a, through Eq. 9. In addition, χ_a varies significantly as a function of pool diameter and mass flow (see Fig. 7). The global model of Orloff and de Ris [6,7] provides burning rate predictions to within a factor of 2 to 3 from experimental results, which may be the best that can be expected using a global approach. It remains unlikely that global models will be able to accurately predict mass vaporization rates for a variety of fuels, over a wide range of pool diameters.

Field models are much more detailed than global models [92]. Rather than one or several zones, these models endeavor to spatially resolve details of the fire structure. Combustion field models are related to the subject known as Computational Fluid Dynamics which is widely used in aerodynamic design. These models typically utilize the k-ε strategy for modeling turbulent transport, which treats turbulence by "time-averaging". This smears-out the transient large scale cyclical structures in the flame which were described in Section 1 [93]. A number of key parameters necessary for accurate k-ε modeling have not been empirically determined for general use and particularly for use in pool fires [94,95]. These parameters, such as the initial turbulence intensity, have a strong impact on the calculated temperature and velocity fields [46].

The key to prediction of mass vaporization rates is proper modeling of radiative transfer to the fuel surface, which is the dominant heat transfer mode for large diameter pool fires. This implies that the time varying distribution of temperature and soot volume fraction must be modeled with some accuracy, especially near the fuel surface. Field models incorporating realistic chemistry (e.g. including the intermediate species, carbon monoxide and molecular hydrogen) have reported physically reasonable calculated flame temperatures [93,96].

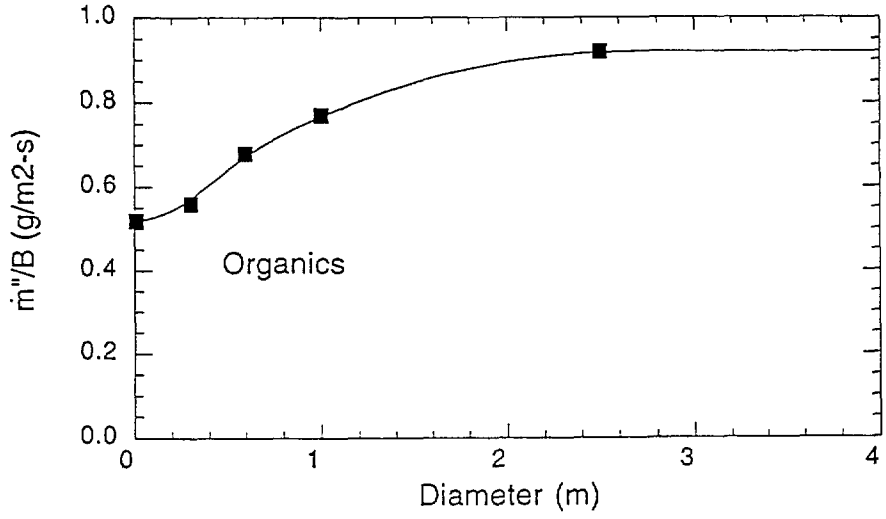

Figure 12 The ratio of the fuel mass flux to the fuel B number ($\dot{m}''/B$) as a function of pool diameter for hydrocarbon fires.

More difficult will be estimation of the soot volume fraction. Even for simple laminar flames, prediction of the soot volume fraction distribution from fundamental kinetics and reduced chemical models has been a challenging problem [97,98]. Only recently has some success been obtained for simple fuels [99].

Recent models using Lagrangian simulations of particle and thermal element trajectories in isothermal plumes [100] and jet flames [101], in conjunction with solutions of the energy and species conservation equations inside each of the reacting thermal elements [102] may provide a reasonable approach for predicting the soot and temperature distributions in pool fires. Simulations of radiative transfer could then determine radiative flux to targets internal or external to the fire [49,103]. Both zone and field models continue to be developed. It is hoped that within the near future these models will provide a basis for prediction of pool fire vaporization rates for varying scale and fuel type. However, much work remains to be completed.

ACKNOWLEDGEMENTS

The authors are very grateful to Professor Jay Gore, Michael Klassen, and Yudaya Sivathanu of Purdue University, Mun Choi and Ishwar Puri of the University of Illinois at Chicago, Katsu Konishi of the Saitama Institute of Technology, and Howard Baum, Paul Borthwick, Andrew Hubbard, Kevin McGrattan, Roy McLane, Holly Rushmeier and John Yang of NIST for technical assistance and many helpful discussions.

REFERENCES

[1] Hall, A.R., Oxidation and Combustion Reviews, **6**, 169 (1973).

[2] Blinov, V.I. and Khudyakov, G.N. (1961). Diffusion Burning of Liquids, Izdatel'stvo Akademii Nauk SSSR, Moscow. English Translation, U.S. Army Engineering Research and Development Laboratories, Information Resources Branch, Translation Analysis Section, Fort Belvoir, VI, No. T-1490a-c.

[3] Bouhafid, A., Vantelon, J.P., Souil, J.M., Bosseboeuf, G., and Rongere, F.X., Fire Safety Journal ,**15**, 367 (1989).

[4] Smith, D.A. and Cox, G., Combust. Flame, **91**, 226 (1992).

[5] Bouhafid, A., Vantelon, J.P., Joulain, P., and Fernandez-Pello, A.C., Twenty-Second Symp. (Int.) on Combust., p. 1291, The Combustion Institute, 1992.

[6] Orloff, L. and de Ris, J., Nineteenth Symp. (Int.) Combust., The Combustion Institute, Pittsburgh, PA, p. 885, 1982.

[7] Orloff, L. and de Ris, J., Froude modeling of pool fires. Factory Mutual Technical Report No. OHON 3.BU RC81-BT-9, Factory Mutual Research, Norwood, MA, 1983.

[8] Beyler, C.L., Ph.D. Dissertation, Harvard University, 1985.

[9] Gengembre, E., Cambray, P., Karmed, D., and Bellet, J.C., Combust. Sci. Tech., **41**, 55 (1984).

[10] Detriche, Ph., and Lanore, J.C., Fire Tech., **16**, 204 (1980).

[11] McCamy, C.S., Paper No. 2678, J. Res. Natl. Bureau of Standards, 293 (1956).

[12] Byram, G.M. and Nelson, R.M., Fire Tech., **6**, 102 (1970).

[13] Portscht, R., Combust. Sci. Tech., **10**, 73 (1975).

[14] McCaffrey, B.J., National Bureau of Standards Internal Report, NBSIR Number 79-1910, 1979.

[15] Baum, H.R. and McCaffrey, B.F., Fire Safety Science-Proceedings of the Second International Symposium. p. 129, 1989.

[16] Weckman, E.J. and Sobiesiak, A., Twenty-Second Symp. (Int.) Combust., The Combustion Institute, p. 1299, 1988.

[17] Zukoski, E.E., Cetegen, B.M. and Kubota, T., Twentieth Symp. (Int.) Combust., The Combustion Institute, p. 361, 1984.

[18] Schonbucher, A., Arnold, B., Banhardt, K., Bieller, V., Kasper, H., Kaufmann, M., Lucas, R., and Schiess, N., Twenty-First Symp. (Int.) on Combust., p. 83, The Combustion Institute, 1986.

[19] Beyler, C.L., Fire Safety J., **11**, 53 (1986).

[20] Sibulkin, M., and Hansen, A.G., Combust. Sci. Tech., **10**, 85 (1975).

[22] Hagglund, B., Fire Res. and Dev. News of Swedish Fire Protection Agency, FoU-Brand **1**, 18 (1977).

[23] Brotz, W., Schonbucher, A., Banhardt, V., and Schiess, N., Ber. Bunsenges. Phys. Chem., **87**, 997 (1983).

[24] Chamberlin, D.S., and Rose, A., The First Symp. (Int.) on Combust., p. 27, The Combustion Institute, 1965.

[25] Barr, J., Fourth Symp. (Int.) on Combust., p. 765, The Williams and Wilkins Co., 1953.

[26] Lamprecht, I., and Schaarschmidt, B., Nature, **240**, 445 (1972).

[27] Pagni, P.J., ASME Paper Number 89-WA/FE-5, p. 26, 1989.

[28] Hamins, A., Yang, J., and Kashiwagi, T., Twenty-Fourth Symp. (Int.) on Combust., p. 1695, The Combustion Institute, (1992).

[29] Chen, L.D., Seaba, J.P., Roquemore, W.M. and Goss, L.P., Twenty-Second Symp. (Int.) on Combust., p. 677, The Combustion Institute, 1988.

[30] Buckmaster, J. and Peters, N., Twenty-First Symp. (Int.) on Combust., p. 1829, The Combustion Institute, 1986.

[31] Bejan, A., J. Heat Transfer, **113**, 261 (1991).

[32] Hertzberg, M., Cashdollar, K., Litton , C., and Burgess, D., The Diffusion Flame in Free Convection, U.S. Bureau of Mines, Report Number 8263, 1978.

[33] Emori, R.I. and Saito, K., Combust. Sci. Tech., **31**, 217 (1983).

[34] Ghoniem, A.F., Personal Communication, Massachusetts Institute of Technology, 1994.

[35] Putnam, A.A., Nature, **192**, 1277 (1961).

[36] Deal, S., Technical Reference Guide for FPETool Version 3.2, National Institute of Standards and Technology report NISTIR 5486, 1994.

[37] McCaffrey, B.J., Flame Height, Chapter 1-18, SFPE Handbook of Fire Protection Engineering, (Ed: P.J. DiNenno), 1988.

[38] Heskestad, G., Fire Safety J. **5**, 103 (1983).

[39] Hasemi, Y., and Nishihata, M., Fire Sci. Tech., **7**, 27 (1987).

[40] Hamins, A., Borthwick, P., Konishi, K., and Kashiwagi, T., Flame Heights of Gaseous Pool Fires, in preparation, (1995).

[41] Heskestad, G., The Eightennth Symp. (Int.) on Combust., The Combustion Institute, p. 951-960, 1981.

[42] Tewarson, A., Smoke Point Height and Fire Properties of Materials, NIST-GCR-88-555, 1988.National Institute of Standards and Technology, available from National Technical Information Service, Springfield, VA 22161, USA.

[43] Delichatsios, M.A., Orloff, L., Delichatsios, M.M., Combust. Sci. Tech., **84**, 199 (1992).

[44] Grosshandler, W.L., RADCAL: A Narrow-Band Model for Radiation Calculations in a Combustion Environment, National Institute of Standards and Technology (NIST) Technical Note 1402, Government Printing Office, Washington, D.C., 1993.

[45] Lee, K.Y., Cha, D.J., Hamins, A., and Puri, I.K., "Heat Release Mechanisms in Inhibited Laminar Counterflow Flames", Combust. Flame, submitted, (1995).

[46] Crauford, N.L., Liew, S.K., and Moss, J.B., Combust. Flame **61**, 269 (1986).

[47] Walker, N.L. and Moss, J.B., Combust. Sci. Tech. **41**, 43 (1984).

[48] Vachon, M. and Champion, M., Combust. Flame **63**, 269 (1986).

[49] Choi, M., Hamins, A., Rushmeier, H., Kashiwagi, T., The Twenty-Fifth Symp. (Int.) on Combust., The Combustion Institute, p. 1471-1480, 1994.

[50] McCaffrey, B.J., Combust. Flame **52**, 149 (1983).

[51] Klassen, M., Sivathanu, Y.R., and Gore, J.P., Combust. Flame, **90**, 34 (1992).

[52] Bilger, R.W., Combust. Flame, **30**, 277 (1977).

[53] Sivathanu, Y. and Faeth, G.M., Combust. Flame, **8231**, 211 (1990).

[54] Jeng, S.M. and Faeth, G.M., ASME Journal of Heat Transfer, **106**, 886 (1984).

[55] Gore, J.P., Ph.D. dissertation, The Pennsylvania State University (1986).

[56] Hamins, A., Kashiwagi, T., Gore, J., and Klassen, M., Combust. Flame, **86**, 223 (1991).

[57] Klassen, M. and Hamins, A., Unpublished Results, (1991).

[58] Koseki, H., Fire Tech. **25**, 241 (1989).

[59] Koseki, H., and Hayasaka, H., Journal of Fire Science **7**, 237 (1989).

[60] Koseki, H., and Yumoto, T., Fire Tech. **24**, 33 (1988).

[61] Yang, J., Hamins, A., and Kashiwagi, T., Combust. Sci. Tech., **96**, 183, 1994.

[62] McCaffrey, B.J., Some measurements of the radiative power output of diffusion flames, Western States Section Meeting, The Combustion Institute, Paper # WSS/CI 81-15 (1981).

[63] Modak, A.T., Factory Mutual Research Corporation, Norwood Massachusetts, Technical Report Serial No. 22361-5, RC-B-67 (1976).

[64] Buch, R., Hamins, A., Borthwick, P., Konishi, K., and Kashiwagi, T., Pool Burning of Siloxane Fluids, in preparation, (1995).

[65] Babrauskas, V., Fire Tech, **19**, 251 (1983).

[66] Mudan, K.S. and Croce, P.A., Fire Hazard Calculations for Large Open Hydrocarbon Fires, Chapter 2-4, SFPE Handbook of Fire Protection Engineering, (Ed: P.J. DiNenno), 1988.

[67] Modak, A., Fire Safety J. **3**, 177 (1981).

[68] Lee, K.Y., Zhong, Z.Y., Tien, C.L., Twentieth Symp. (Int.) on Combust., p. 1629, The Combustion Institute, 1984.

[69] Kung and Stavriandus, Nineteenth Symp. (Int.) on Combust., p. 905, The Combustion Institute, 1982.

[70] American Society of Testing and Materials, D-1322, Standard Test Method for Smoke Points of Aviation Turbine Fuels, 1975, (Re-approved 1980).

[71] Nakakuki, A., Combust. Flame **96**, 311 (1994).

[72] Arpaci, V.S. and Selamet, A., Combust. Flame, **86**, 203 (1991).

[73] de Ris, J. and Orloff, L., Combust. Flame, **18**, 381 (1972).

[74] Corlett, R.C., Combust. Flame, **14**, 351 (1970).

[75] Hottel, H.C., Fire Research Abstracts Reviews, **1**, 41 (1959).

[76] Burgess, D. and Hertzberg, M., In Heat Transfer in Flames, (Eds.: N.H. Afgan and J.M. Beers), John Wiley & Sons, New York, NY, Chapter 27, 1974.

[77] Orloff, L., Eighteenth Symp. (Int.) Combust., The Combustion Institute, Pittsburgh, PA, p. 549, 1981.

[78] Mudan, K.S., Prog. Energy Combust. Sci., **10**, 59, (1984).

[79] de Ris, J., Seventeenth Symp. (Int.) on Combust., p. 1003, The Combustion Institute, (1979).

[80] Blinov, V.I. and Khudyakov, G.N., Dokl. Acac. Nauk SSSR **117**, 1094 (1957).

[81] Hamins, A., Klassen, M., Gore, J., Fischer, S., and Kashiwagi, T., Combust. Sci. Tech., **96**, 37 (1994).

[82] Akita, K. and Yumoto, T., Tenth Symposium (Int.) on Combust, p. 943, The Combustion Institute, 1965.

[83] Corlett, R.C. and Fu, T.M., Pyrodynamics, **4**, 253 (1966).

[84] Modak, A. and Croce, P.A., Combust. Flame **30**, 251 (1977).

[85] Yumoto, T., Combust. Flame **17**, 108 (1971).

[86] Shinotake, A., S. Koda and K. Akita, Combust. Sci. Tech., **43**, 85 (1985).

[87] Alger, R.S., Corlett, R.C., Gordon, A.S., and Williams, F.A., Fire Tech **15**, 142 (1979).

[88] Spalding, D.B., Fourth Symp. (Int.) on Combust., p. 1847, The Combustion Institute, 1952.

[89] Kanury, A.M., Introduction to Combustion Phenomena, Chapter 4, Gordon and Breach Science Publishers, Langhorne, PA, 1975.

[90] Spalding, D.B., Some Fundamentals of Combustion, Batterworth, London, England, 1955.

[91] Hayasaka, H., and Koseki, H., Estimation of thermal radiation from large pool fires. 11th Joint Meeting of the UJNR Panel on Fire Research and Safety, Berkeley, CA, 1989.

[92] Cox, G., In Fire Science in Technology, (Eds. F. Weichung and F. Zhuman), International Academic Publishers, Hefei, China, p. 50, 1992.

[93] Nicolette, V.F., Tieszen, S.R., Gritzo, L.A., Moya, J.L.,Cornell, G., Annual Conference on Fire Research, Gaithersburg, MD, October, 1994, National Institute of Standards and Technology internal report #NISTIR 5499, p.83, 1994.

[94] Bilger, R.W., Fire Safety Science-Proceedings of the Fourth International Symposium. p. 95, 1994.

[95] Adiga, K.C., Raemaker, D.E., Tatem, P.A., and Williams, F.W., Fire 6Safety J., **14**, 241 (1989).

[96] Holen, J., Brostrom, M., and Magnussen, B.F., Twenty-Third Symp. (Int.) on Combust., p. 1677, The Combustion Institute, 1990.

[97] Kent, J.H. and Honnery, D.R., Combust. Flame, **79**, 287 (1990).

[98] Kennedy, I. M. and Kollman, W., Combust. Flame, **81**, 73 (1990).

[99] Leung, K.M., Linstadt, R.P. and Jones, W.P., Combust. Flame, **87**, 289 (1991).

[100] Baum, H.R., Ezekoye, O.A., McGrattan, K.B., and Rehm, R.G., Theoret. Comput. Fluid Dynamics, **6**, 125 (1994).

[101] Jang, J.H., Sivathanu, Y.R., and Gore, J.P., Heat and Mass Transfer in Fire and Combusting Systems, **HTD-223**, 81 (1992).

[102] Zhang, Z, and Ezekoye, O.A., Computational Study of State Relationships for Acetylene-Air Diffusion Flames with Soot Radiation, to be presented at the National Heat Transfer Conference, Portland, OR, 1995.

[103] Klassen, M., Gore, J.P., Sivathanu, Y.R., Hamins, A., and Kashiwagi, T., Twenty-Fourth Symp. (Int.) on Combust., p. 1713, The Combustion Institute, 1992.